Journal of Agrometeorology

(A publication of Association of Agrometeorologists)

ISSN : 0972-1665 (print), 2583-2980 (online)

Vol. No. 28 (3) :302-313 (September - 2026)

https://doi.org/10.54386/jam.v28i3.3484

https://journal.agrimetassociation.org/index.php/jam

Research paper

Multi Index Climate Drought Assessment (MICDA) Using Hybrid ML Weightings – A Spatio temporal analysis for the Semi-Arid Watershed in Eastern Ghats, India (2000–2024)

SATHISH KUMAR BALACHANDRAN and SIVAKUMAR RAMAMOORTHY*

Department of Civil Engineering, College of Engineering and Technology, SRM Institute of Science and Technology, Kattankulathur, Chengalpattu, Tamil Nadu, India

**Corresponding author email: sivakumr@srmist.edu.in*

ABSTRACT

Reliable drought assessment at the watershed scale remains challenging because individual drought indicators often capture only specific dimensions of drought and does not represent the combined influence of meteorological, hydrological, and vegetation-related stressors. A comprehensive Combined Drought Index (CDI) for the ARG watershed (1,186.23 km²) using Principal Component Analysis (PCA), ML models, and multi-decadal remote-sensing data (2000-2024) was carried out. Six drought indicators SPI_3, ETA, VHI, SMAI, MNDWI, and FAPAR were used for CDI generation. CDI weights were calculated using PCA driven Random Forest (RF) and Multiple Linear Regression (MLR) model. RF showed superior performance (R = 0.887; r^2 = 0.786). Spatiotemporal analysis shows 7 of 25 years with drought conditions, associated with high temperatures (34-36°C) and unpredictable monsoon precipitation (<1000 mm). The drought analysis in the catchment and command area along with trend analysis shows recovery patterns. The long-term satellite data was used for scalable drought monitoring for Multi Indicator Climate Drought Assessment (MICDA). The PCA–RF-based CDI supports Sustainable Development Goals SDG-6, SDG-13, and SDG-15 by utilizing data to plan for watershed resilience and monitor drought in real time.

Keywords: Combined Drought Index (CDI), Remote sensing, PCA, RF, MLR, Google Earth Engine, Geo-informatics framework.

Drought is a severe climatic hazard that occurs when there is a prolonged period of low precipitation, increased evapotranspiration demand, poor vegetation health, low soil moisture, and limited surface water availability. In contrast, it advances gradually as a result of intricate interactions among water, agriculture, and weather phenomena (Kannan *et al.,* 2025). This leads to serious damage to the environment and stress on the economy, especially in areas that depend on farming. Numerous studies suggest that drought is one of the most devastating and not widely recognized natural calamities. Increasing climate change is worsening its frequency and intensity (Berhail & Katipoğlu, 2024). Significant rainfall changes, higher temperature extremes, and water loss through evaporation make drought dynamics worse in monsoon-heavy countries like India. Most meteorological droughts begin with a lack of rain, which leads to an agricultural drought when soil moisture is depleted and plants are stressed. Finally, a hydrological drought reduces streamflow and groundwater (Hao *et al.,* 2017). Therefore, climate-driven assessment methodologies are essential. Conventional drought assessments have relied on the precipitation indices (SPI and SPEI) or vegetation-centric indices. These indices are advantageous for illustrating certain characteristics of drought, but they rarely represent how drought impacts multiple areas simultaneously.

According to studies, vegetation indices may not effectively represent drought severity when heat stress or soil moisture restrictions are the main drivers, which represent agricultural and ecological dryness. Thus, recent research has highlighted the need for multi-index drought assessment frameworks that include meteorological, hydrological, and vegetation-based indicators to better capture drought complexity (Yu *et al.,* 2019; Bera *et al.,* 2025). Remote sensing provides reliable, spatially

Article info - DOI: *https://doi.org/10.54386/jam.v28i3.3484*

Received:20 April 2026; Accepted: 07 July 2026; Published online : 7 September 2026

detailed, and extended land surface observations, making it an effective multi-index drought monitoring technique. Vegetation health indicators, land surface temperature, soil moisture proxies, evapotranspiration and water indices derived from satellite images have been extensively utilized for monitoring agricultural and ecological drought in different climates.

Research in India and other semi-arid regions shows that collective remote sensing indices better explain drought variations across time and geography than single-index techniques. Multi-collinearity, redundancy, and ranking variable significance can occur when many drought indicators are used (Mondal *et al.,* 2024). By lowering dimensionality and identifying dominating drought indicators from linked multi-index datasets, PCA has been widely used to address these issues (Parthsarthi Pandya *et al.,* 2022). PCA based CDI capture the dominant drought stress variability while preserving the physical interpretability of each indicator. PCA focuses on linear correlations, and it may not show how climatic factors, vegetation response, and soil moisture dynamics interact non-linearly.

Recent research has shown the environmental benefits of hybrid frameworks that use statistical dimensionality reduction and machine learning (ML) models to overcome these challenges. Machine-learning techniques, especially ensemble approaches like Random Forest (RF), are good in assessing drought severity (Prasad *et al.,* 2025). RF can describe non-linear interactions in high-dimensional datasets and remain strong when data is inconsistent (Kanji & Das, 2025). For regional and watershed drought characterization and prediction, hybrid ML approaches outperform regression-based methods. One of the most climate-vulnerable parts of southern India is the Eastern Ghats region. It has erratic monsoon rains, significant evapotranspiration, and severe temperatures. Because of the geography, land use, and soil characteristics, sub- and milli-watersheds in this area, especially those at hill–plain transitions, respond differently to drought (Gumma *et al.,* 2019; Kulkarni *et al.,* 2020). Despite their importance for regional water security and agriculture's long-term health, watershed scale MICDA are rare.

To address the challenges of the single indicator-based drought assessment, this study establishes a Multi-Indicator Climate Drought Assessment (MICDA) framework for the ARG watershed by integrating multi-decadal remote sensing datasets, PCA and machine learning techniques in a cloud-computing environment. The objectives of this study are:

(i) To characterize the spatio-temporal variability of drought conditions in the ARG watershed during 2000–2024 using meteorological, hydrological, agricultural, and vegetation-based drought indicators.

(ii) To develop a PCA-driven machine learning framework for adaptive indicator weighting and Combined Drought Index (CDI) generation.

(iii) To analyze drought dynamics in the catchment and command and to study long-term drought trends for watershed scale drought monitoring and climate-resilient water resource planning.

MATERIALS AND METHODS

Study Area

The Aiyar–Rudhrakombai–Gundur (ARG) watershed is a medium-sized basin located in the Eastern Ghats region of Tamil Nadu, southern India, lies between 10°53′40″–11°25′04″ N and 78°29′40″–78°34′50″ E, covering an area of approximately 1,186.23 km². The watershed exhibits diverse physiographic characteristics, with about 32% comprising steep terrain, including portions of the Kolli Hills (16.95%) and Pachamalai Hills (12.31%), while the remaining area consists predominantly of gently sloping plains. The elevation varies from 52 m in the command region to 1,384 m in the catchment region, resulting in notable changes in the landscape that affect runoff, infiltration, and the variability of water flow (Fig. 1). The drainage network comprises of seasonal streams connected to the Cauvery River system, converging near the Mukkombu dam. Approximately 30.83 km² of lakes and ponds support groundwater recharge and local water storage, although their capacity declines during prolonged dry periods. The region experiences a semi-arid tropical climate with annual rainfall ranging from 800 to 1,600 mm, primarily driven by the Northeast monsoon (October–December), while the Southwest monsoon contributes relatively less precipitation.

Land use is dominated by agriculture (~70%), with forests covering about 18% of the watershed. Agricultural productivity is highly sensitive to rainfall variability and evapotranspiration demand. The combined effects of complex terrain, monsoon dependence, and intensive land use result in pronounced spatial variability in drought occurrence, making the ARG watershed a suitable case for multi-indicator drought assessment.

Methodology

The methodological framework of this study is to develop a Multi-Index Climate–Drought Assessment (MICDA) through an integrated PCA and Machine Learning (ML) is illustrated in Fig. 2.

Data Source

This study utilized hydro-climatic and satellite-derived datasets from GEE that covered 2.5 decades, from 2000 to 2024. Table 1 contains drought classifications, indicators, and satellite dataset sources for computing CDI. Cloud masking, temporal filtering, and anomaly screening were used to understand the indicators consistency over the timeline (Paul et al., 2025). The watershed boundary was delineated using SOI 1:50,000 toposheet and ASTER DEM drainage networks. Which was utilized for spatial masking to restrict analysis to the research region.

The proposed framework delineates drought phases by integrating hydro-climatic and remote sensing-based indicators. SPI_3 monitors short-term precipitation anomalies and illustrates how monsoonal variability fosters drought (Prasad *et al.,* 2025). ETA balances atmospheric demand and moisture supply to relate temperature extremes to surface water stress (Vicente-Serrano *et al.,* 2010). SMAI reveals root zone moisture loss preceding

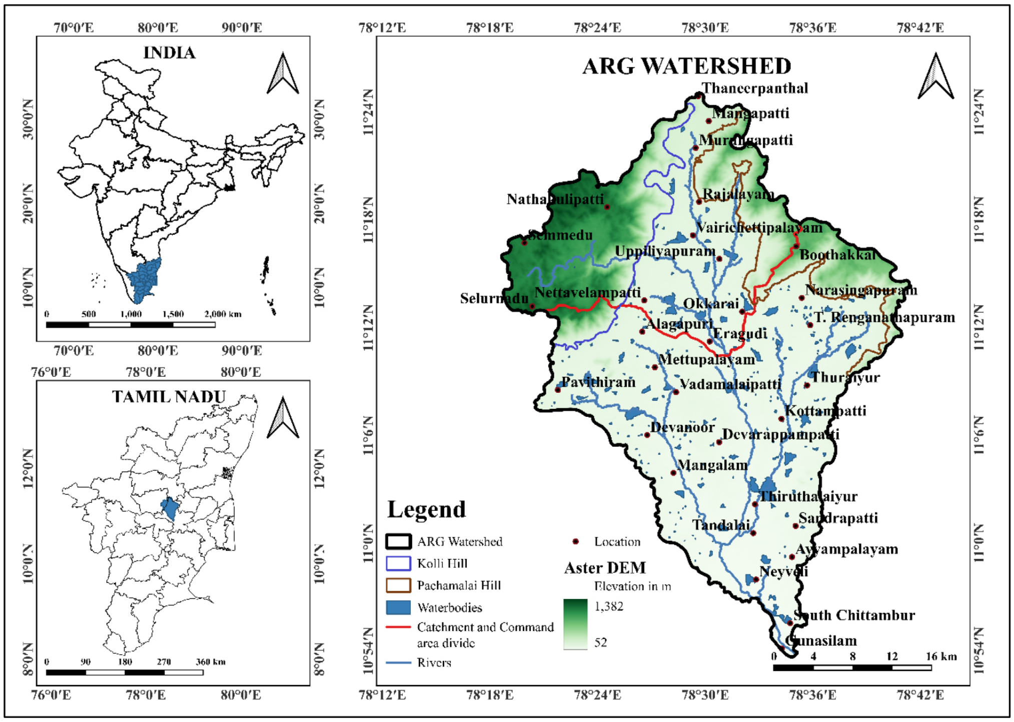

Fig. 1: Study area - ARG watershed

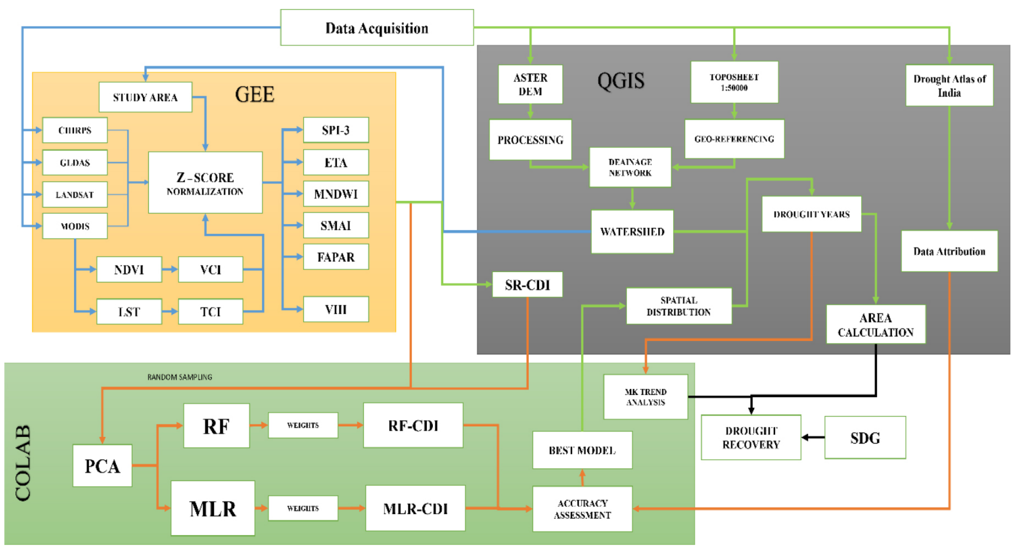

Fig. 2: Methodology Flowchart

agricultural drought. MNDWI evaluates surface water availability and desiccation of tanks, lakes, and small reservoirs, which are critical during extended droughts. These factors indicate climate and hydrology that progress watershed drought (Patil *et al.,* 2024).

Vegetation-based indicators measure ecological and agricultural climatic stress. The VHI tracks how drought and rising land temperature influence crops and vegetation (Burka *et al.,* 2024). The FAPAR shows that drought stress reduces vegetative output and photosynthetic efficiency (Giridharan & Sivakumar 2024; Zhang *et al.,* 2025). Vegetation and moisture indicators increase drought, whereas meteorological conditions cause it. These indicators help to analyse drought as a multi-dimensional process, that includes rainfall deficiency, soil moisture depletion, vegetation stress, and surface water decrease. The drought index SPI_3 was computed by fitting the three-month cumulative precipitation totals to a gamma probability distribution and transformed to standard normal distribution (Mckee *et al.,* 1993).The resulting SPI_3 was used to describe the short-term meteorological drought conditions within the study area. On the other hand, ETA, SMAI, MNDWI, and FAPAR were estimated from their source datasets and normalised using Eq. (1) before multivariate integration (Cabello-Solorzano *et al.,* 2023).

$$Z_i = \frac{(X_i - \mu_m)}{\sigma_m} \quad (1)$$

Table 1: Drought indicators and its data source

Drought Type	Indicators	Satellite Data
Meteorological	SPI_3 (Standardized Precipitation Index)	CHIRPS
Hydrological	MNDWI (Modified Normalized Difference Water Index)	MODIS (MOD09A1) surface reflectance
	SMAI (Soil Moisture Anomaly Index)	GLDAS (NOAH v2.1)
	FAPAR (Fraction of Absorbed Photosynthetically Active Radiation)	MODIS (MOD15A2H and MCD15A3H V6.1)
Agricultural	ETA (Evapotranspiration Anomaly)	MOD16A2 v6.1 global evapotranspiration datasets
	VHI (Vegetation Health Index)	MOD11A2 for Land Surface Temperature (LST) and MOD13Q1 for Normalized Difference Vegetation Index (NDVI)

$$VCI = \frac{(NDVI - NDVI_{min})}{(NDVI_{max} + NDVI_{min})} \tag{2}$$

$$TCI = \frac{(LST_{max} - LST)}{(LST_{max} + LST_{min})} \tag{3}$$

$$VHI_y = \alpha * \left(\sum_{i=1}^{n} \frac{VCI_i}{n}\right) + (1 - \alpha) * \left(\sum_{i=1}^{n} \frac{TCI_i}{n}\right) \tag{4}$$

Where, X_i = observed value for a certain parameter, μ_m = mean for month m across the years 2000 to 2024, σ_m = standard deviation for month m (long term baseline), α = weighting coefficient (0.5 for equal influence of both indices). VHI is a derived index from VCI and TCI which was generated based on NDVI and LST using Eq. (2) and Eq. (3) (Liu & Kogan 1996; Burka *et al.,* 2024). The VHI was calculated using α = 0.5, assigning equal weights to VCI and TCI following the original formulation proposed by Kogan, (1995). This approach has been widely adopted in drought-monitoring studies and provides a balanced representation of vegetation and thermal stress during drought assessment. VHI was subsequently computed using Eq. (4) and standardized to maintain consistency with the other drought indicators. The normalization process transforms all observations into dimensionless anomalies, facilitating integrated PCA–machine learning analysis of meteorological and biophysical drought conditions.

Integration of PCA with Machine Learning for Weight Derivation

An annual Synthetic Raster (SR) layer was generated for each year from 2000 to 2024 by spatially integrating the standardized drought indicators using Eq. (5). The resulting SR represented the composite drought condition of the watershed based on the combined influence of all normalized indicators. To reduce spatial clustering, a fixed set of 4750 spatially random sample points was generated for every year and each indicator to capture spatial variability in the watershed. Those sample points were maintained constant throughout the study period. It supports the spatially representative sampling of multi-indicator data for robust statistical and ML analysis. A 4750 × 6 matrix was created from the observations for each year, with columns representing standardized drought indicators and rows representing spatial samples.

$$SR = \frac{SPI_3 + SMAI + FAPAR + MNDWI + ETA + VHI}{6} \tag{5}$$

PCA was used to reduce dimensionality and indicates redundancy in this dataset. The top two PCs (PC1 and PC2) out of the six PCs explaining ≥ 80% of total variance were kept, and eigenvalues and eigenvectors were analysed to determine each indicator's contribution to the dominant variance structure (Parthsarthi Pandya *et al.,* 2022). Using Google Colab, both PCA and ML techniques were implemented. For model training, the SR was the dependent variable and the PC1 and PC2 were the independent variables. Random Forest (RF) and Multiple Linear Regression (MLR) models were used to calculate the weight coefficients for every year separately.

The RF and MLR coefficients are based on the PCs rather than the original indicators, hence those coefficients cannot be used directly as weights for the indicators. At that point, the eigenvector relationships were used to back-calculate indicator weights from model outputs to the original indicators for each year. Finally, the obtained values were then normalized to a total of one for all indicator weights (Table 2). These normalized weights were then used to generate the yearly CDI using Eq. (6) with the contributions of the indicators (Mondal *et al.,* 2024).

$$CDI = (W_{SPI3} * SPI_3) + (W_{SMAI} * SMAI) + (W_{FAPAR} * FAPAR) + (W_{MNDWI} * MNDWI) + (W_{ETA} * ETA) + (W_{VHI} * VHI) \tag{6}$$

MLR was used as a baseline model with interpretable linear relationships, while RF was used due to its robustness to multicollinearity and ability to model complex nonlinear interactions (Wang *et al.,* 2022). Evaluation of model performance included Coefficient of determination (r^2), correlation coefficient (R), Mean Absolute Error (MAE), and Root Mean Squared Error (RMSE). The 2000–2020 Drought Atlas of India Standardized Precipitation Evapotranspiration Index (SPEI) was used for external validation (Chuphal *et al.,* 2024). Further the 2021–2024 extended CDI dataset was created using the best model.

The SR was only used as an internal composite representation of the integrated drought conditions, and the target variable for weight derivation. The purpose of the RF and MLR models was not to provide predictive forecasting, but rather to determine the proportional impact of drought indicators by adaptive weighting. To reduce the possibility of circularity, the resultant CDI was independently validated against the Drought Atlas of India (DAI) SPEI dataset, rather than the SR itself.

Spatio-Temporal Drought Assessment and Trend Analysis

In the ARG watershed, yearly CDI maps from 2000 to 2024 were used to assess drought trends. Spatial analysis identifies

Table 2: Example for PCA driven RF model weight calculation (2016)

Indicators	Input		Weight calculation				
	PC1	PC2	PC1*RF_1	PC2*RF_2	Sum	|Sum|	Weights
FAPAR	0.073	0.063	0.065	0.007	0.072	0.072	0.049
ETA	-0.019	-0.020	-0.017	-0.002	-0.019	0.019	0.013
MNDWI	0.208	0.465	0.184	0.054	0.238	0.238	0.161
SMAI	0.939	-0.333	0.830	-0.039	0.791	0.791	0.534
SPI_3	0.259	0.818	0.229	0.096	0.324	0.324	0.219
VHI	-0.041	0.007	-0.036	0.001	-0.035	0.035	0.024
PCA-RF	0.883	0.116				1.479	1

Table 3: Drought Severity Classification

CDI Range	Drought Severity Index
CDI ≥ 1.5	Very wet
1.0 ≤ CDI < 1.5	Moderately wet
0.5 ≤ CDI < 1.0	Slightly wet
0 ≤ CDI < 0.5	Damp
-0.5 ≤ CDI < 0	Moderately damp
-0.8 ≤ CDI < -0.5	Abnormal drought
-1.3 ≤ CDI < -0.8	Moderate drought
CDI < -1.3	Severe drought

drought intensity and persistence, whereas temporal analysis evaluates inter-annual drought variability. To maintain homogeneity in drought severity interpretation, CDI values were classified using conventional drought categories from existing frameworks (Mckee *et al.,* 1993; Kogan, 1995) and linked with the Drought Atlas of India (Chuphal *et al.,* 2024). Minor changes were made to harmonise categorization criteria across indicators. Table 3 represent the drought severity classification according to CDI. The variability with respect to monsoonal rainfall variations and temperature conditions were examined to determine how precipitation deficiencies and increased evapotranspiration cause drought.

The non-parametric Mann–Kendall (MK) test was conducted to assess the statistical significance of these patterns in hydro-climatic time series. Sen's slope estimator was used to measure CDI monotonic trends to analyse long-term drought dynamics. The combination of spatio-temporal evaluation and trend analysis yields a comprehensive evaluation of drought intensity and geographical dispersion. This enables long term drought analysis using MICDA and aids in drought risk assessment at the watershed level, which was directly integrated with Sustainable Development Goals (SDG-6, SDG-13, and SDG-15).

RESULT AND DISCUSSION

This study highlights the application of the MICDA framework for the ARG watershed using PCA driven ML models. The spatio-temporal variability of drought is investigated through the analysis of various drought indicators in relation to rainfall and temperature, emphasizing their collective impact on drought severity. The analysis underscores the benefits of a multi-indicator approach that incorporates meteorological, agricultural, and vegetation-based variables, in contrast to single-indicator SPEI.

Inter-Correlation Analysis of Drought Indicators

The correlation matrix supports drought indicator-meteorological factor relationships under hydrological stress (Table 4). It shows that precipitation anomalies affect watershed vegetation and surface energy exchange. FAPAR positive correlations with SPI_3 (R = 0.501) and SMAI (R = 0.489) show that soil-moisture availability strongly affects photosynthetic efficiency and vegetation productivity, indicating that vegetation response is closely linked to short-term meteorological fluctuations. The subsurface hydro MNDWI showed modest positive associations with SPI_3 (R = 0.383) and rainfall (R = 0.367), indicating precipitation variability affects surface-water availability. Although weaker than the SPI_3–rainfall connection (R = 0.800), lakes, ponds, and drainage networks react more slowly to rainfall shortages via storage and runoff.

The weak correlation between MNDWI and SMAI (R = 0.118) suggests that surface-water extent and root-zone soil moisture are governed by different hydrological pathways, while the near-zero correlation with FAPAR (R = 0.017) suggests that open-water availability does not directly control vegetation productivity. Temperature negatively correlates with VHI, ETA, and rainfall, worsening drought symptoms by increasing evapotranspiration losses and vegetation thermal stress (Patil *et al.,* 2024). These associations suggest that interrelated meteorological, hydrological, and biological processes regulate drought dynamics in the ARG watershed, justifying the inclusion of MNDWI as a supplemental hydrological indicator in the multi-indicator CDI framework.

The relationships show that drought dynamics in the ARG watershed is managed by an integrative hydro-climatic process in which rainfall deficits cause stress and increasing temperature promotes moisture loss and vegetation degradation. This integrated correlation approach provides the hydrological foundation for PCA-driven modeling and machine learning methods, allowing drought management to account climatic variables throughout time.

Model Validation and CDI Interpretation

In comparison to the SPEI (Drought Atlas of India) data, the RF model surpassed the MLR model, attaining a good r^2 of 0.786 relative to MLR (r^2 = 0.629) (Fig. 3). The RF model exhibited a better correlation (R = 0.887) in contrast to MLR (R = 0.793), signifying enhanced coherence with observed drought conditions (Table 5). Regarding error metrics, RF exhibited a lower RMSE (0.910) compared to MLR (0.933), indicating better results in capturing extreme variations, whereas MAE values were

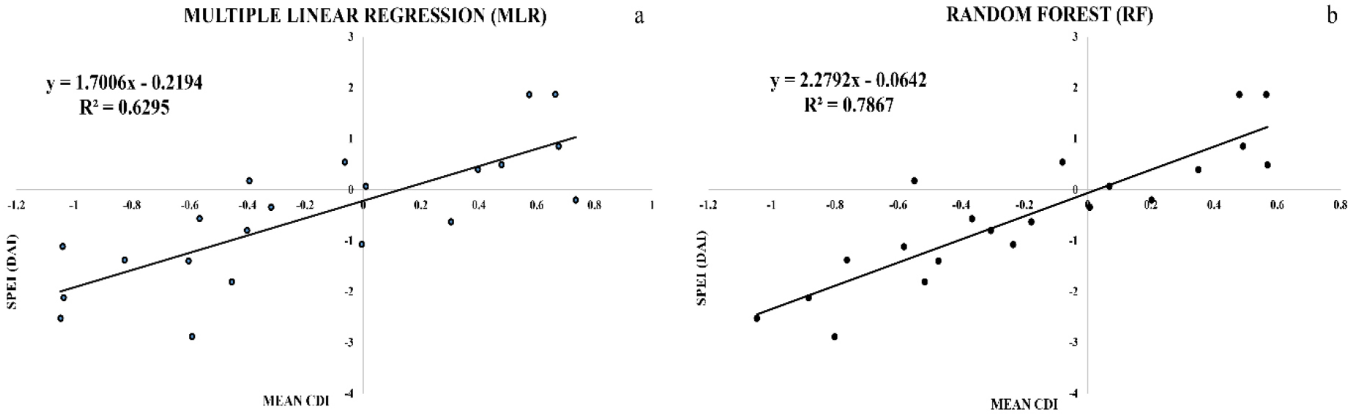

Fig. 3: Coefficient of determination of ML model (2000 – 2020); a. MLR; b. RF

Table 4: Correlation analysis between the drought indicators, rainfall and temperature**.**

Indicators	SPI_3	SMAI	ETA	FAPAR	MNDWI	VHI	Rainfall	Temperature
SPI_3	1							
SMAI	0.489	1						
ETA	0.346	0.338	1					
FAPAR	0.501	0.532	0.417	1				
MNDWI	0.383	0.118	0.251	0.017	1			
VHI	0.578	0.327	0.647	0.353	0.338	1		
Rainfall	0.800	0.347	0.60	0.470	0.367	0.658	1	
Temperature	-0.561	-0.432	-0.699	-0.370	-0.185	-0.840	-0.582	1

nearly similar (RF = 0.734; MLR = 0.710). The better efficiency of RF illustrates its capacity to identify nonlinear correlations and extensive relationships among drought indicators, whereas MLR offers a fundamental linear analysis of drought behaviour (Wang *et al.,* 2022).

Table 5: ML model performance metrics

Model	R	RMSE	MAE
PCA–RF	0.887	0.91	0.7349
PCA–MLR	0.793	0.933	0.710

However, its limited explanatory power indicates that drought processes in the ARG watershed is influenced by non-linear interactions among climate variables, vegetation response, and soil moisture dynamics. The PCA pre-processing improved model stability by reducing multi-collinearity among input indicators, thus benefiting both modeling approaches. Finally, the CDI was calculated using equation (6).

The RF model was further used for weights identification and temporal extension of CDI from 2021 to 2024. The RF-derived CDI values were analyzed to determine the drought years according to a threshold of CDI < −0.5, which indicates the drought conditions. According to Table 3, seven years from 2000 to 2024 were identified as experiencing drought (Fig. 4). Notable drought years are 2002 (−0.801), 2003 (-0.516), 2009 (−0.762), 2012 (−0.548), 2014 (−0.582), 2016 (−0.883) and 2017 (-1.047). In this scenario, 2017 exhibited the most extreme drought conditions during the study period, succeeded by 2016 and 2002.

Spatio-Temporal Analysis

Spatio-temporal drought dynamics in the ARG watershed were assessed by integrating RF-CDI, drought indicators, rainfall, and temperature (Fig. 1). Between 2000 and 2020, the Drought Atlas of India (DAI) recognized 11 drought years using SPEI (< −0.5) as the drought threshold (Table 3). RF-CDI identified seven drought years 2002, 2003, 2009, 2012, 2014, 2016 and 2017 with good agreement with consistent negative anomalies across the indicators (Fig. 4).

These drought years witnessed reduced rainfall (739.8–1027.1 mm), increased temperatures 33–36°C, and substantial drops in SPI_3, VHI, SMAI, and ETA, suggesting meteorological, agricultural, and hydrological stress (Fig. 5). Continuously negative MNDWI values indicate surface water shortages (Fig. 6). The classic drought phenomenon starts from insufficient rainfall to soil dryness and vegetation being stressed and becomes more severe by high temperatures that increase ETA demand (Bhuiyan & Kogan, 2010; Dakhil *et al.,* 2026).

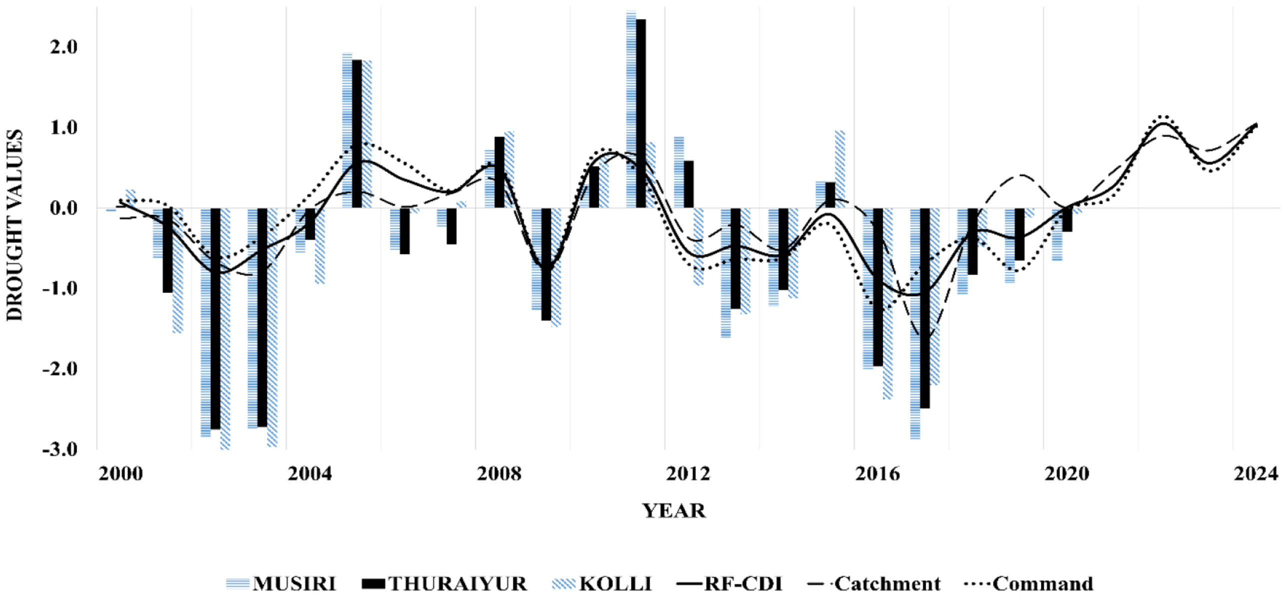

Fig. 4: CDI distribution over the years

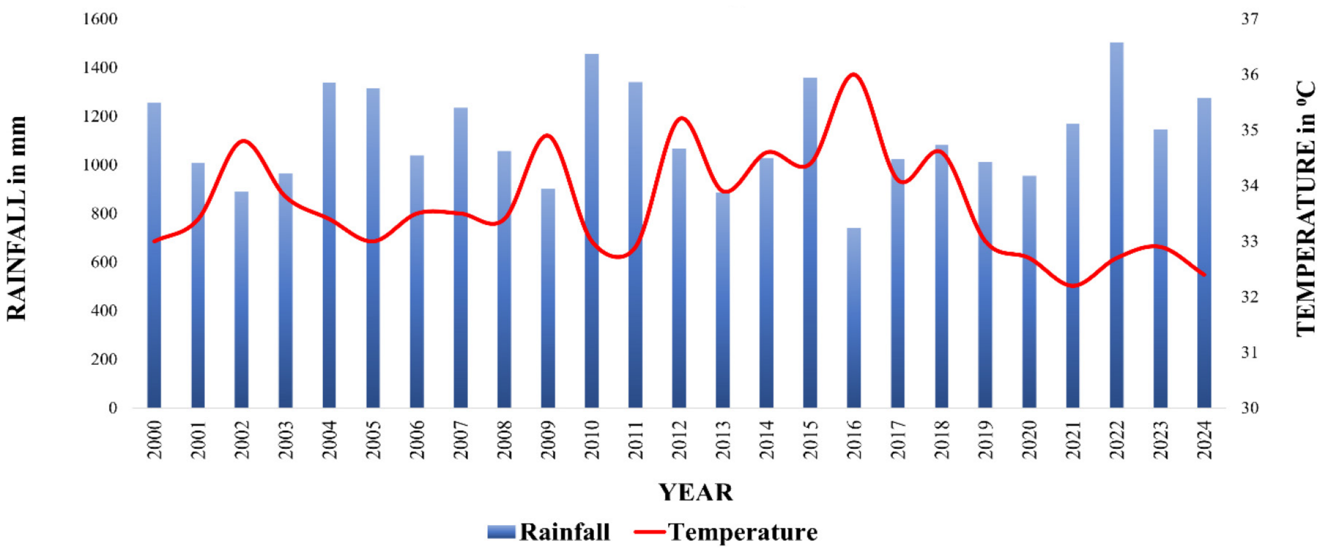

Fig. 5: Distribution of rainfall and temperature over the years

Conversely, DAI recognised 2012 (0.173) as a non-drought year whereas the CDI (-0.548) was identified as abnormal drought category that owing to localised or short-term stress (Fig. 4), were soil moisture recovery or vegetative resistance attenuated drought consequences.

SPEI-based evaluations may represent temporary meteorological anomalies, while CDI measures integrated hydro-climatic stress. The substantial association between CDI, rainfall, temperature, and drought indicators emphasizes the need for multi-indicator drought assessment and focused watershed management. The spatial distribution of drought years is illustrated along with its post monsoon satellite image in Fig. 7.

Catchment Area Drought Analysis

The catchment area of the ARG watershed is 451.06 km² that includes part of the Kolli and Pachamalai Hills. It indicates that the area is very sensitive to temperature-induced drought, even though it receives over 800-1,200 mm of rain a year. The elevation of 115–1382 m and temperature range of 23–39°C increase surface runoff and evapotranspiration (Fig. 5). This decreases soil moisture retention and increases dryness. CDI assessed 2002 (-0.668), 2003 (-0.786), 2009 (-0.791), 2014 (-0.517) and 2017 (-1.622) as drought occurred years in catchment area, suggesting meteorological drought and agricultural and hydrological stress. Over 75% of the upper catchment experienced moderate to severe drought, with

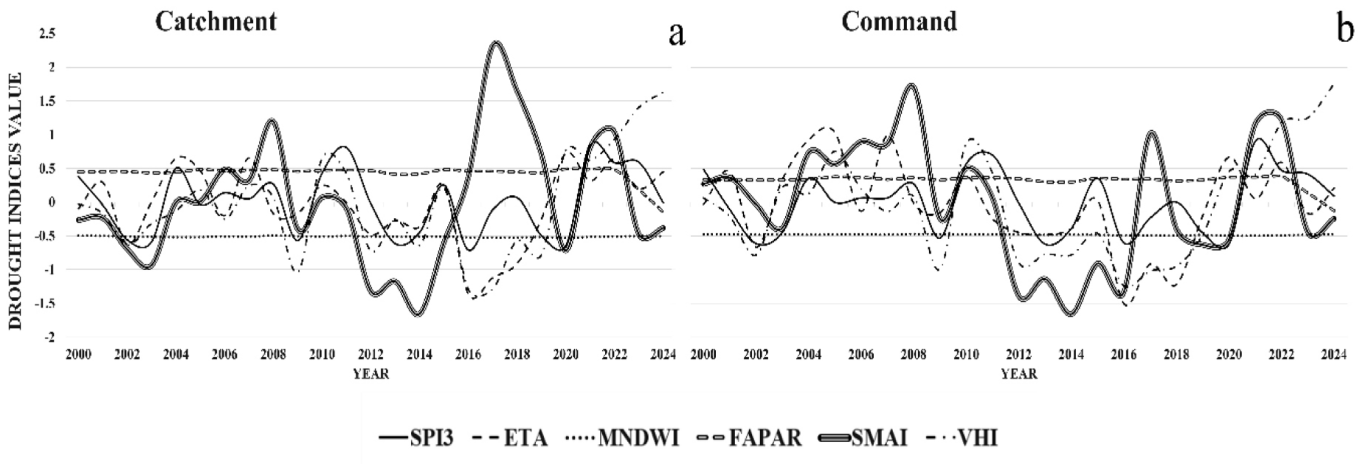

Fig. 6: Distribution of drought indicators **a.** Catchment; **b.** Command

approximately 84% impacted in 2002, indicating hydro-ecological stress. The propagating process is seen in indicator responses.

The 2003 drought was caused by precipitation deficiency, soil moisture depletion, and vegetation stress. Low rainfall (<1000 mm) and high temperatures range between 32°C and 37°C led to significant negative anomalies in SPI_3, MNDWI, VHI, and SMAI (Fig. 6). The areas mainly Manmalai, Adakkampudu Kombai, Gundurnadu, Thinnanur, and Devanur were badly affected.

A severe drought conditions persisted in 2017 with temperatures between 33°C and 38°C. Significant surface water stress (−0.525) along with severe ETA depletion (-1.124) and vegetation deterioration (−1.29) indicate continued agricultural and hydrological dryness due to short-term rainfall unpredictability. This affected the areas of Okkarai, Venkatachalapuram, Poolambadi RF., Sirunavalur, and Uppiliapuram villages (Fig. 7). However, the CDI did not define 2001 as a meteorological drought year, unlike the DAI. Vegetation, evapotranspiration, and a positive FAPAR of 0.453 and ETA of 0.29 limited drought propagation (Fig. 6). The differences show that precipitation shortfalls, temperature stress, soil moisture persistence, and vegetation resistance affect drought in catchment area.

Command Area Drought Analysis

The ARG watershed oversees 737.94 km² of downstream plains impacted by river confluences, surface-water storage, and irrigation. Unlike the upper catchment, the command region has moderate climatic fluctuation, with annual rainfall between 750 and 1400 mm and temperature variations of 31°C to 39°C, making it more resilient to short-term meteorological droughts.

The command area demonstrated a more intense and frequent occurrence of drought compared to the catchment region. The years characterized by significant drought in the command area were 2002 (-0.606), 2009 (-0.744), 2012 (-0.696), 2013 (-0.636), 2014 (-0.622), 2016 (-1.256), 2017 (-0.693), and 2019 (-0.775). These drought occurrences align with the meteorological drought conditions shown in the DAI dataset. For an instance, the years 2002, 2014 and 2016 were exhibiting annual precipitation below 1000 mm and mean temperatures over 34°C, reflecting the synergistic impacts of precipitation shortfalls and elevated atmospheric water demand.

The negative CDI values throughout these years correlated with substantial soil moisture depletion in 2014 of -1.66 and 2016 -1.328, reduced evapotranspiration activity of -0.669 in 2002 and -1.51 in 2016 associated with pronounced vegetative stress -0.782, -0.781 and -1.239. Decreased rainfall availability led to negative SPI_3 of -0.615, -0.389 and -1.256 along with deteriorating surface water conditions of MNDWI less than -0.45. The effects of drought were particularly significant in the villages of Kannanur, Eragudi South, Neiveli, T. Renganathapuram, Kombai, Pavithram Pudhur, Devanur, Alagapuri, and Urakkarai. This indicates the susceptibility to recurrent hydro-climatic stress.

Despite 2001 and 2006 being moderate drought years by the DAI, the command area's CDI values above the drought threshold are due to positive FAPAR, SMAI, and evapotranspiration response. Hydrological buffering and land-surface responses may have limited drought propagation in these places.

In 2012, although DAI classified the year as damp which infers as a non-meteorological drought, but the CDI identifies the drought conditions. This observation suggests the presence of agricultural and hydrological stress which was not recognized by the precipitation-based indices (SPEI). Despite the rainfall exceeding 1000 mm with SPI_3 value of -0.017, the high mean temperature of 35°C along with negative evapotranspiration (-0.449), severe soil moisture depletion (-1.392) and severe vegetation stress of -0.901. This indicates that the region was prone to soil moisture limitations and temperature- driven drought intensification

Extreme years show considerable regional diversity in abnormal to severe intensity classes over the command-area. Drought affected 95.36% of the watershed in 2002, 89.43% in 2014, and 96.45% in 2012 and 74.03% in 2016, indicating watershed has a wide hydro-climatic stress. It validates widespread agricultural and hydrological drought based on DAI meteorological extremes.

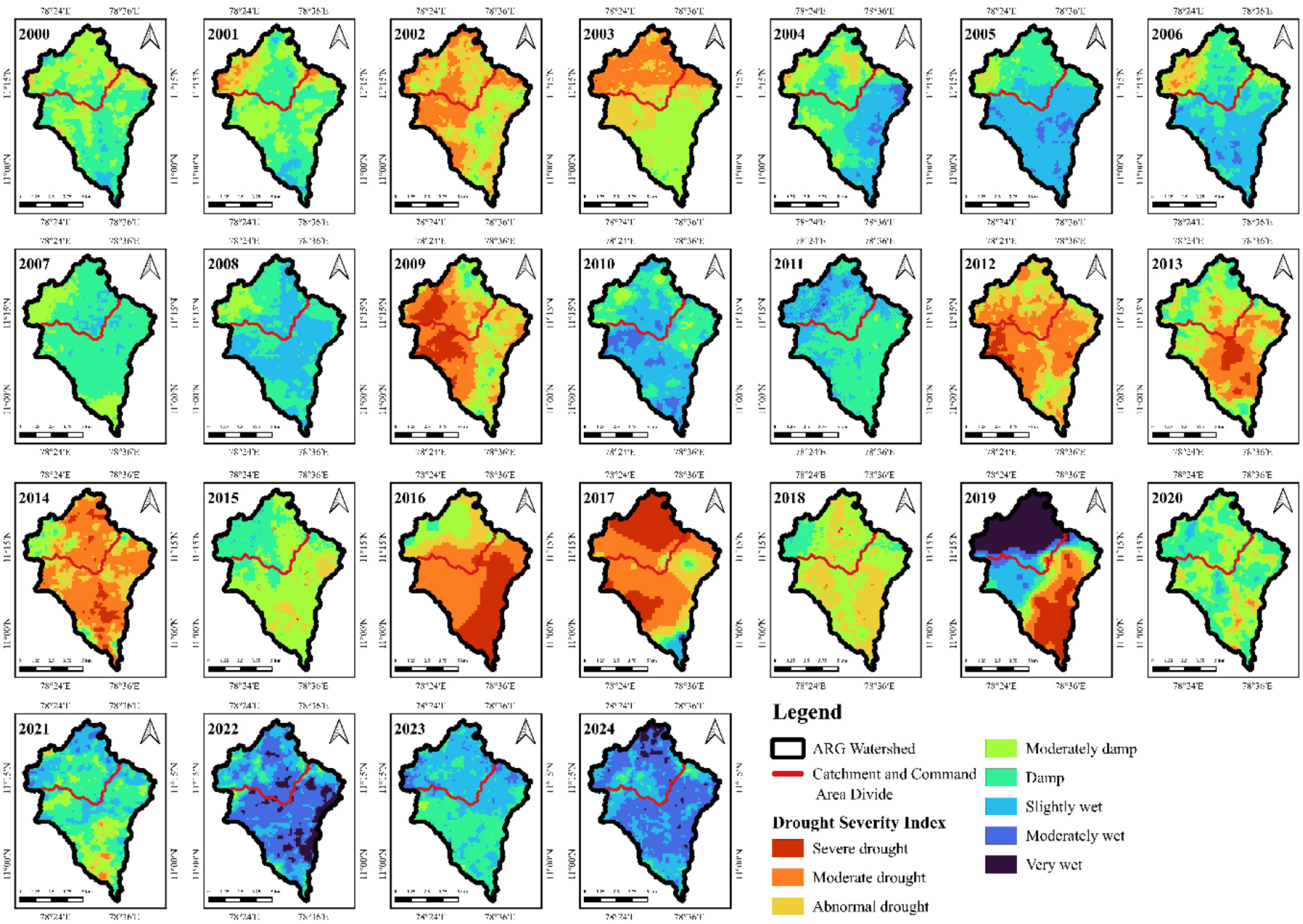

Fig. 6: Distribution of drought indicators a. Catchment; b. Command

Trend Analysis

Trend analysis was performed using the Mann–Kendall test and Sen's slope estimator at α = 0.05, exhibited unique drought patterns across the catchment and command regions. The catchment exhibited a significant positive trend ($\tau = 0.327$, $p = 0.0223$, Sen's slope = 0.039 yr^{-1}) showing a change from drought-dominated circumstances in the early 2000s to generally wetter conditions in subsequent years (Fig. 8a). The change of CDI values from negative to positive is additional evidence of hydro-climatic recovery (Fig. 6a). This change leads to better vegetation and moisture conditions, as illustrated by higher VHI, FAPAR and soil moisture. Field findings indicate that the increased plantations and step agriculture in the Kolli Hills and extensive forest cover in the Pachamalai Hills could have contributed to enhanced ecosystem resilience and moisture retention.

Conversely, the command area did not exhibit a statistically significant long-term trend ($\tau = 0.027$, $p = 0.871$, Sen's slope = 0.006 yr^{-1}), despite a modest positive Sen's slope. This suggests that drought variability is predominantly influenced by inter-annual climatic fluctuations rather than sustained recovery (Fig. 8b). Although the Aiyar river system provides seasonal water (Fig. 8b: i), the negative MNDWI values over time imply inadequate surface water storage and recurrent water stress (Fig. 8b: ii). The drying of lakes and ponds is projected to restrict the availability of water for agriculture. Localized use of drip irrigation helps preserve vegetation health and evapotranspiration (Fig.8b: iii). These inconsistent reactions of indicators account for the lack of a substantial recovery trend in the command area.

The integrated spatio-temporal study shows that rainfall triggers droughts, whereas temperature-induced evapotranspiration stress, plant health, and soil moisture dynamics affect severity and extent. This framework may be adopted for the semi-arid regions with similar terrain conditions. The hybrid PCA–RF-based MICDA framework for climate-sensitive drought evaluation can be further improved by using high resolution satellite images and microclimate data that may help to identify drought in sub-watershed scale.

The framework supports the SDG 6 (Clean Water and Sanitation) with specific reference to Target 6.4. It helps effective planning of water use and identification of drought prone zones which would aid in improved allocation of limited and restricted water resources. It is also associated with SDG 13 (Climate Action) especially Target 13.1 by observing hydro-climatic variability using continuous long-term satellite data and machine learning methods to enhance adaptive capacity and resistance to climate-related disasters. Moreover, the presence of vegetation indicators (VHI and FAPAR) helps to SDG 15 (Life on Land), particularly Target

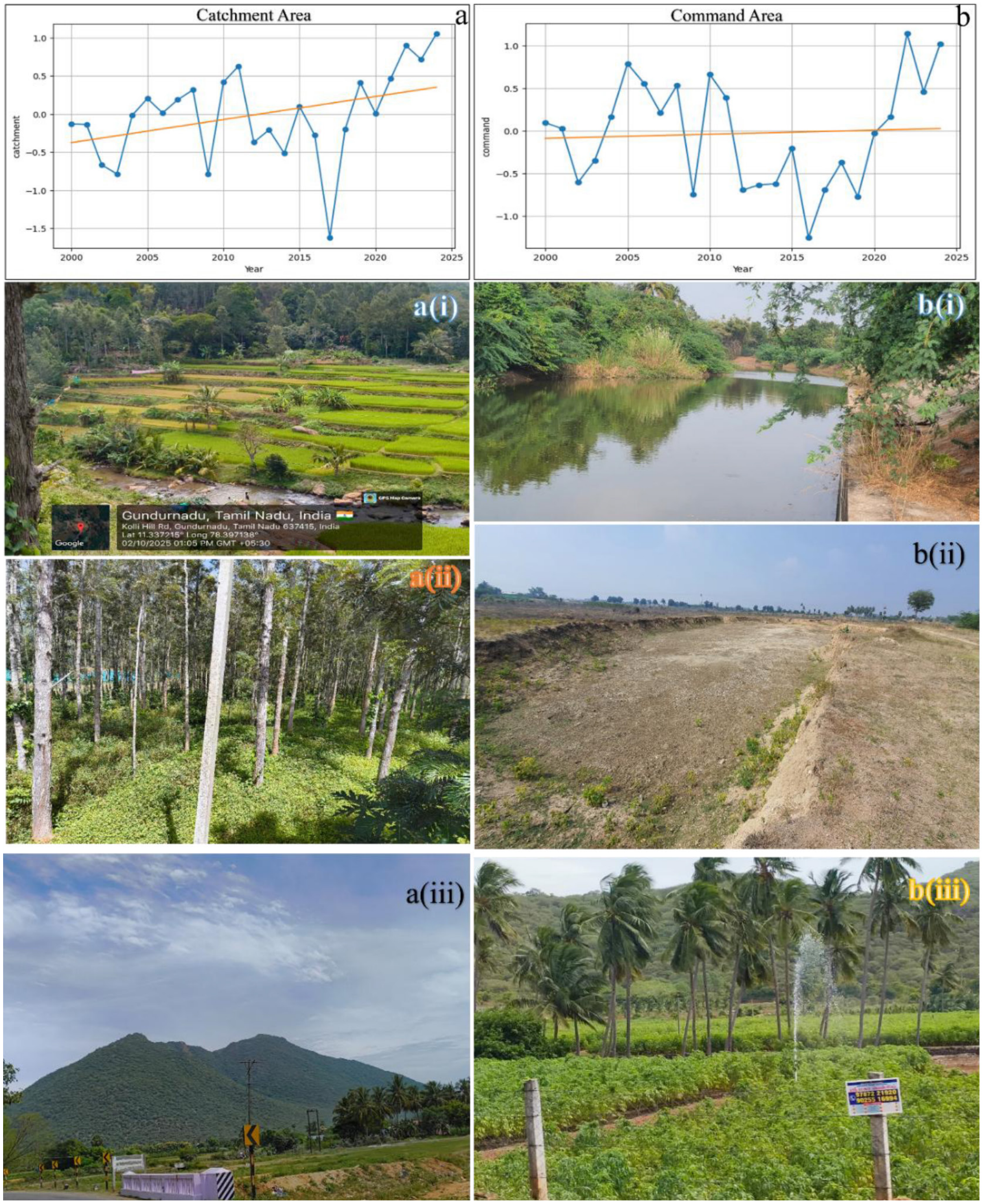

Fig. 8: Trend analysis and Field images (NE-monsoon 2025): a. Catchment, (i) Step cultivation fields in Kolli hill, (ii) Plantation in Kolli hills, (iii) Forest cover over Pachaimalai hill; b. Command, (i) Aiyar River near Konakkarai, (ii) Dried Sithambur lake, (iii) Drip irrigation in Tuber crop field near Uppiliyapuram

15.3, by allowing the measurement of ecosystem stress and land degradation processes in semi-arid environments. In summary, the MICDA framework proposes a scalable and data-driven approach to drought monitoring, risk reduction and climate resilient watershed management.

CONCLUSION

This study demonstrates that drought dynamics in the ARG watershed is influenced not only by precipitation deficits but also by temperature-induced evapotranspiration, soil moisture, and vegetation response. The hybrid PCA–RF framework effectively captured these interactions, explaining about 80% of the variance. RF ($r^2 = 0.786$) did better than MLR. The years 2002, 2003, 2009, 2012, 2014, 2016 and 2017 were major drought years, which shows the spreading of hydro-climatic stress across the watershed. Droughts were episodic and affects over 60–90% of area over the watershed. The catchment and command regions exhibited distinct drought characteristics. The command area experienced a greater frequency of drought events, reflecting its susceptibility to prolonged hydro-climatic stress, whereas the catchment area showed a significant positive recovery trend and improved moisture conditions over time. These contrasting responses highlight the importance of region-specific drought management strategies within the watershed. The ML integrated CDI is a tool that can be used to monitor droughts in real time and manage watersheds that associated with SDG 6, SDG 13, and SDG 15.

ACKNOWLEDGMENT

The authors would like to express gratitude to SRM Institute of Science and Technology Kattankulathur for the support and providing the necessary facilities in Earthquake Research Cell (EQRC) to complete the research

Author's certificate: The manuscript or its part is not under consideration for publication elsewhere and the same has been approved by all co-authors.

Conflict of Interests: The authors declare that there is no conflict of interest regarding the publication of this article.

Funding: This research received no external funding.

Data Availability: The original contributions presented in this study are included in the article. Further inquiries can be directed to the corresponding author.

Author's contribution: **Sathish Kumar Balachandran:** Involved in data collection and methodology, writing, and original draft preparation; **Sivakumar Ramamoorthy:** Contributed to supervision, process, review, and resources.

Disclaimer: The contents, opinions, and views expressed in the research article published in the Journal of Agrometeorology are the views of the authors and do not necessarily reflect the views of the organisations they belong to.

Publisher's Note: The periodical remains neutral concerning jurisdictional claims in published maps and institutional affiliations.

REFERENCES

Bera, D., Dutta, D., Poddar, S., & Kundu, A. (2025). Meteorological drought dynamics and climatic interactions in the arid and semi-arid regions of western India. *Journal of Environmental Management,* 387, 125836. https://doi.org/10.1016/j.jenvman.2025.125836

Berhail, S., & Katipoğlu, O. M. (2024). Exploring hydrological and meteorological drought trends in Northeast Algeria: Implications for water resource management. *Theoretical and Applied Climatology,* 155, 9689–9712. https://doi.org/10.1007/s00704-024-05207-y

Bhuiyan, C., & Kogan, F. N. (2010). Monsoon variation and vegetative drought patterns in the Luni Basin in the rain-shadow zone. *International Journal of Remote Sensing,* 31, 3223–3242. https://doi.org/10.1080/01431160903159332

Burka, A., Biazin, B., & Bewket, W. (2024). Spatial drought occurrences and distribution using VCI, TCI, VHI, and Google Earth Engine in Bilate River Watershed, Rift Valley of Ethiopia. *Geomatics, Natural Hazards and Risk,* 15. https://doi.org/10.1080/19475705.2024.2377672

Cabello-Solorzano, K., Ortigosa de Araujo, I., Peña, M., et al. (2023). The impact of data normalization on the accuracy of machine learning algorithms: A comparative analysis. *Lecture Notes in Networks and Systems,* 750, 344–353. https://doi.org/10.1007/978-3-031-42536-3_33

Chuphal, D. S., Kushwaha, A. P., Aadhar, S., & Mishra, V. (2024). Drought atlas of India, 1901–2020. *Scientific Data,* 11. https://doi.org/10.1038/s41597-023-02856-y

Dakhil, F. T., Sabtu, N. B., & Khalaf, A. G. (2026). Assessment of agricultural and meteorological drought in Southern Iraq's wetlands using vegetation condition and drought indices. *Journal of Agrometeorology,* 28(1), 32–37. https://doi.org/10.54386/jam.v28i1.3161

Giridharan, N., & Sivakumar, R. (2024). Estimation and monitoring on fraction of absorbed photosynthetically active radiation (FPAR) changes in Sathyamangalam Reserve Forest. *Lecture Notes in Civil Engineering,* 398, 215–226. https://doi.org/10.1007/978-981-99-6229-7_18

Gumma, M. K., Nelson, A., & Yamano, T. (2019). Mapping drought-induced changes in rice area in India. *International Journal of Remote Sensing,* 40, 8146–8173. https://doi.org/10.1080/01431161.2018.1547456

Hao, C., Zhang, J., & Yao, F. (2017). Multivariate drought frequency estimation using copula method in Southwest China. *Theoretical and Applied Climatology,* 127, 977–991. https://doi.org/10.1007/s00704-015-1678-5

Kanji, S., & Das, S. (2025). Assessing predictability of spatio-temporal soil-moisture heterogeneity with satellite-data using GeoDetector and ensemble machine learning models considering environmental and climatic factors. *Journal of Hydrology,* 663, 134312. https://doi.org/10.1016/j.jhydrol.2025.134312

Kannan, P. R. G., Govindasamy, R., & Radhika Panchabikesan, V. A. (2025). Hydrological drought assessment using drought indices in semi-arid zones of Vaippar river sub basins, Tamil Nadu, India. Theoretical and Applied Climatology, 156, 519. https://doi.org/10.1007/s00704-025-05766-8

Kogan, F. N. (1995). Application of vegetation index and brightness temperature for drought detection. *Advances in Space Research,* 15, 91–100. https://doi.org/10.1016/0273-1177(95)00079-T

Kulkarni, S. S., Wardlow, B. D., Bayissa, Y. A., Tadesse, T., Svoboda, M. D., & Gedam, S. S. (2020). Developing a remote sensing-based combined drought indicator approach for agricultural drought monitoring over Marathwada, India. *Remote Sensing,* 12. https://doi.org/10.3390/rs12132091

Liu, W. T., & Kogan, F. N. (1996). Monitoring regional drought using the vegetation condition index. *International Journal of Remote Sensing,* 17, 2761–2782. https://doi.org/10.1080/01431169608949106

Mckee, T. B., Doesken, N. J., & Kleist, J. (1993). The relationship of drought frequency and duration to time scales. *In Proceedings of the Eighth Conference on Applied Climatology,* (pp. 17–22).

Mondal, S., Arun Prasad, K., Balasubramani, K., & Kaliraj, S. (2024). Assessment of agricultural drought severity in the Southern Agroclimatic Region of Tamil Nadu using remote sensing-based combined drought index. In 2024 IEEE India Geoscience and Remote Sensing Symposium (InGARSS 2024). *Institute of Electrical and Electronics Engineers.*

Parthsarthi Pandya, N., Gontia, N. K., & Parmar, H. V. (2022). Development of PCA-based composite drought index for agricultural drought assessment using remote sensing. *Journal of Agrometeorology,* 24(4), 384–392. https://doi.org/10.54386/jam.v24i4.1738

Patil, P., Jagtap, M. P., & Dakhore, K. K. (2024). Drought severity estimation using NDWI index in Parbhani district of Maharashtra. *Journal of Agrometeorology,* 26(2), 225–227. https://doi.org/10.54386/jam.v26i2.2540

Prasad, A., Singh, R. K., Ramana Rao, K. V., & Saxena, C. K. (2025). Applicability of machine learning models for drought prediction using SPI in Kalahandi, Odisha. *Journal of Agrometeorology,* 27(2), 216–220. https://doi.org/10.54386/jam.v27i2.2906

Vicente-Serrano, S. M., Beguería, S., & López-Moreno, J. I. (2010). A multiscalar drought index sensitive to global warming: The standardized precipitation evapotranspiration index. Journal of Climate, 23, 1696–1718. https://doi.org/10.1175/2009JCLI2909.1

Wang, Q., Zhao, L., Wang, M., Wu, J., Zhou, W., Zhang, Q., & Deng, M. (2022). A random forest model for drought monitoring and validation for grassland drought based on multi-source remote sensing data. *Remote Sensing,* 14, 4981. https://doi.org/10.3390/rs14194981

Yu, H., Li, L., Zhu, W., Piao, D., Cui, G., Kim, M., Jeon, S., W., & Lee, W. K. (2019). Drought monitoring of the wetland in the Tumen River Basin between 1991 and 2016 using Landsat TM/ETM+. *International Journal of Remote Sensing,* 40, 1445–1459. https://doi.org/10.1080/01431161.2018.1524604

Ssembajwe, R., Twah, A., Kagezi, G. H., Loytty, T., Kobusinge, J., Gidudu, A., Arinaitwe, G., Du, Q., & Voda, M. (2025). Assessment and validation of FAPAR, a satellite-based plant health and water stress indicator, over Uganda. *Remote Sensing,* 17(20), 3501. https://doi.org/10.3390/rs17203501